An investigation of the flow dependence of temperature gradients near large vessels during steady state and transient tissue heating

Michael C Kolios†‡, Arthur E Worthington†, David W Holdsworth§,
Michael D Sherar‖ and John W Hunt†

† Division of Experimental Therapeutics, The Ontario Cancer Institute and Department of
Medical Biophysics, University of Toronto, 610 University Avenue, Toronto, Ontario M5G-2M9,
Canada
§ Imaging Research Laboratories, Robarts Research Institute, London, Ontario N6A 5K8, Canada
‖ Division of Medical Physics, The Ontario Cancer Institute and Department of Medical
Biophysics, University of Toronto, 610 University Avenue, Toronto, Ontario M5G-2M9, Canada

Abstract. Temperature distributions measured during thermal therapy are a major prognostic factor of the efficacy and success of the procedure. Thermal models are used to predict the temperature elevation of tissues during heating. Theoretical work has shown that blood flow through large blood vessels plays an important role in determining temperature profiles of heated tissues. In this paper, an experimental investigation of the effects of large vessels on the temperature distribution of heated tissue is performed. The blood flow dependence of steady state and transient temperature profiles created by a cylindrical conductive heat source and an ultrasound transducer were examined using a fixed porcine kidney as a flow model. In the transient experiments, a 20 s pulse of hot water, $30\,°C$ above ambient, heated the tissues. Temperatures were measured at selected locations in steps of 0.1 mm. It was observed that vessels could either heat or cool tissues depending on the orientation of the vascular geometry with respect to the heat source and that these effects are a function of flow rate through the vessels. Temperature gradients of $6\,°C\,mm^{-1}$ close to large vessels were routinely measured. Furthermore, it was observed that the temperature gradients caused by large vessels depended on whether the heating source was highly localized (i.e. a hot needle) or more distributed (i.e. external ultrasound). The gradients measured near large vessels during localized heating were between two and three times greater than the gradients measured during ultrasound heating at the same location, for comparable flows. Moreover, these gradients were more sensitive to flow variations for the localized needle heating. X-ray computed tomography data of the kidney vasculature were in good spatial agreement with the locations of all of the temperature variations measured. The three-dimensional vessel path observed could account for the complex features of the temperature profiles. The flow dependences of the transient temperature profiles near large vessels during the pulsed experiments were consistent with the temperature distributions measured in the steady state experiments and provided unique insights into the process of convective heat transfer in tissues. Finally, it was shown that even for very short treatment times (3-20 s), large vessels had significant effects on the tissue temperature distributions.

1. Introduction

Thermal therapies utilize the cytotoxic effects of high or low temperatures to destroy pathological tissue. Procedures that rely on raising tissue temperature above $40–41\,°C$

‡ Present address: Department of Math, Physics and Computer Science, Ryerson Polytechnic University, Toronto, Ontario M5B 2K3, Canada.

may be classified into high-temperature thermal therapy in which tissues are exposed to temperatures between 50 and 90 °C for short periods of time (10 min–3 s) or mild temperature hyperthermia in which tissues are exposed to lower temperatures (40–45 °C) for longer time periods (30 min–several hours). Clinical trials of hyperthermia as an adjuvant to radiation therapy have demonstrated that thermal parameters measured during the treatments are linked to treatment outcome (Sherar *et al* 1997, Hand *et al* 1997, Kapp 1996, Kapp and Cox 1995). Furthermore, lesion dimensions produced by high-temperature thermal therapy correlate well with predictions based on calculating transient temperature distributions (Kolios *et al* 1996, Damianou *et al* 1995, Hill *et al* 1994). Therefore, it is important to understand the determinants of temperature distributions in heated tissues to optimize and assess the efficacy of these therapies.

Temperature distributions measured during hyperthermia treatments are often heterogeneous, leading to poorly heated tissues and/or patient discomfort due to hot spots and possible burning. The temperature distributions depend primarily on three factors: (a) the power deposition pattern of the heating source, (b) tissue heat conduction and (c) convective heat transfer by blood flow. Blood flow cooling is the least well understood of these factors, even though clinical (Levin *et al* 1994), experimental (Rawnsley *et al* 1994, Kolios *et al* 1994, Dorr and Hynynen 1992) and theoretical (Kolios *et al* 1995, Crezee and Lagendijk 1992, Roemer 1991, Lagendijk 1982) studies have demonstrated the importance of blood flow in determining the temperature distributions during hyperthermia. A better understanding of how blood flow affects the temperature distributions of heated tissues would help in improving thermal therapy treatment planning and optimizing the design of applicators for heating perfused tissues.

The effects of blood flow can be either localized (i.e. large temperature gradients occurring over small tissues volumes) or regional (i.e. smaller gradients occurring over large tissue volumes). Localized temperature gradients are attributed to heat transport by large vessels ($\geqslant$0.5 mm in diameter, also termed thermally significant vessels) as they traverse a heated volume (Chato 1980). To calculate heat transfer by these vessels, an additional advective term is added to the heat conduction equation (Huang *et al* 1996, Kotte *et al* 1996, Arkin *et al* 1994, Dutton *et al* 1993). The advective term models forced convection heat transfer by blood moving through the vessels. While the physics of heat transfer by forced convection is the same for smaller vessels, these vessels cannot induce significant localized temperature gradients in tissue. Collectively, however, they influence the temperature distributions by cooling over larger scales (regional cooling). In this paper, however, only temperature gradients near thermally significant vessels will be explored. The analysis of temperature profiles in the absence of thermally significant vessels is presented elsewhere (Kolios *et al* 1998).

There is a substantial body of theoretical work that demonstrates the effects of large vessels on the temperature distributions of heated tissues. However, there is a paucity of experimental data that correlate temperature profile variations with vascular geometry. Raaymakers *et al* (1998) examined steady state temperature profiles of heated excised bovine tongues and compared the temperature distributions with a generic three-dimensional discrete vessel model of the bovine tongue, demonstrating qualitative agreement between theory and experiment. Rawnsley *et al* (1994) demonstrated experimentally the effect of large vessels on a heated greyhound thigh *in vivo* and correlated the spatial location of temperature gradients with 2D x-ray angiography images. In this study discrete vessels were added retrospectively, guided by the imaging, so that their simulated temperature distribution matched the experimental data. Dorr and Hynynen (1992) used ultrasonic pulses to demonstrate the effect of a 5 mm diameter vessel on the temperature rise *in vivo*. In these studies parameters such as blood flow rate, temporal changes in flow and the positioning of thermocouples and source were difficult to control. Moreover, few studies have addressed the effects of variables such as vessel flow rate,

counter-current heat exchange and heat source geometry in controlled laboratory experiments. Finally, the temperature gradients caused by the same vascular geometry for steady state and transient tissue heating have not been compared. The specific goals of this paper are to: (a) measure temperature gradients near thermally significant vessels as a function of flow in a controlled manner; (b) correlate the spatial location of the thermally significant vessels as determined by angiography with densely sampled temperature profiles; and (c) measure and compare the effects of the thermally significant vessels for steady state and transient heating for the same vascular and heating geometries. Finally, we examine if perturbations in the temperature distribution caused by large vessels are affected by the power deposition pattern of the heating source.

In these studies, a fixed porcine kidney was used as the perfused tissue model. A hot water needle and ultrasound transducer were the two energy sources used to heat the kidney. The hot water needle was used to model the localized heating of interstitial applicators while the ultrasound transducer represented more regional heating. By controlling renal artery inflow, the flow dependence of steady state and transient temperature profiles was recorded. Computed tomography angiography was performed after the heating experiments to obtain the large vessel geometry in the kidney. The location of the vessels with respect to the heating source and the thermocouples was recorded and compared with the locations of localized heating and cooling detected in the temperature profiles for both the steady state and transient experiments. Examination of the flow dependence of the tissue temperature response to a 20 s pulse of hot water provided a better understanding of the convective properties of large vessels and heat transfer between vessels.

2. Experimental methods

2.1. Thermometry and heating method

An 80 g fixed porcine kidney was used as a perfusion model according to the protocol developed by Holmes *et al* (1984) and modified by Jia (1995). In this procedure, the organ is fixed such that the vasculature retains its integrity allowing it to be used as a flow phantom when perfused *ex vivo*. X-ray images using iodine contrast agents and temperature pulse-decay experiments confirmed that the mass and thermal clearance mechanisms were not compromised (Jia 1995).

The kidney was perfused with distilled deionized water controlled by a computerized peristaltic pump (Masterflex, model 7550-600, Barrington, IL, USA) connected to a pressure meter (DRUCK GLA Electronica 86-20, Milan, Italy), bubble trap and filter (Milipore Corporation, Bedford, MA, USA) (figure 1). Kidney perfusate was circulated through a heat exchanger located in the waterbath to ensure that the perfusate and waterbath temperatures were equal. Inflow pressure was limited to a maximum of 125 mmHg to avoid vascular damage. To achieve low flows (<2.5 ml min^{-1}), the peristaltic pump was disconnected and a needle valve was included in the circuit to accurately adjust flow. Circuit pressure differential was achieved by using a water reservoir elevated by 1.85 m from the kidney level as indicated in figure 1. Volumetric flow for the low-flow experiments was measured using a graduated cylinder and stopwatch. The experimental set-up is similar to that used by Crezee and Lagendijk (1990) in bioheat transfer experiments in the bovine kidney.

The kidney was immersed in a waterbath at room temperature. The waterbath was stirred by connecting it to a circulation circuit (flow rate $\simeq 4$ l min^{-1}) and a thermocouple was used to measure the waterbath temperature. The heat source consisted of an 18-gauge (1.2 mm outer diameter) needle perfused with hot water (at temperature T_{in}) to induce temperature gradients in the tissue. The source temperatures T_{in} ranged from 40–50 °C for the steady state
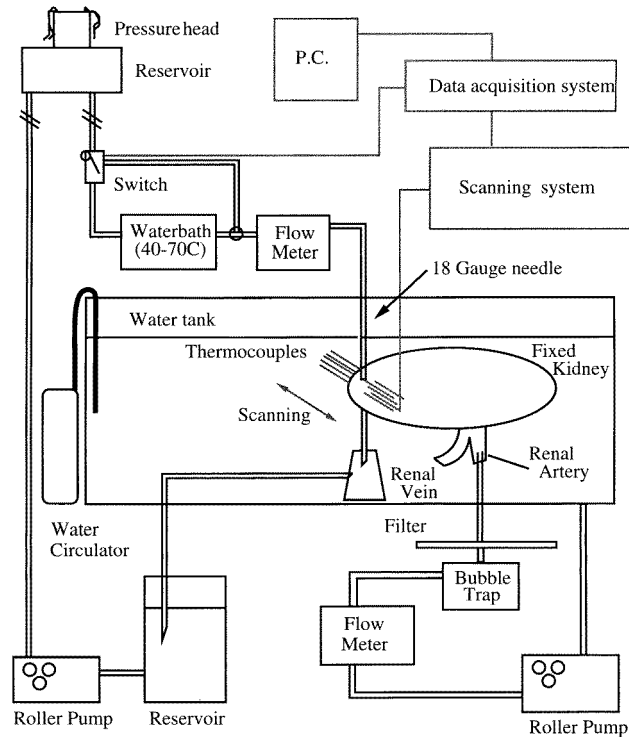
Figure 1. The experimental system built to examine temperature distributions in a heated kidney as a function of flow. It consists of four main components: two flow circuits (for the kidney and the heat source), a scanning system and a thermometry data acquisition system. Five thermocouples are scanned in steps of 100 μm, providing high spatial resolution measurements.

experiments and 60–70 °C for the transient experiments. The temperature of the water was monitored at the entry and exit points of the needle. Needle flow was achieved by use of the water reservoir discussed previously (volumetric flow through needle $\simeq$1.2 ml s^{-1}). Steady state temperature profiles were collected for all thermocouples along a length of 40 mm in the kidney for a series of renal artery inflows ranging from 0 to 45 ml min^{-1}. For the transient experiments, a computer controlled pinch valve (Cole Parmer, part H-98301-22, Chicago, USA) was used to switch between hot and room-temperature water to deliver a 20 s heat pulse to the kidney. The experimental protocol is shown schematically in figure 2(*a*). To accelerate kidney cooling before stepping the thermocouples to another location, the kidney inflow was set to 40 ml min^{-1} for 20–30 s after data acquisition. Pre-selected regions of the kidney were scanned to reduce acquisition time. Each 8 mm kidney scan (in steps of 0.1 mm) took approximately 3 1/2 h to complete.

Five type K chromel alumel thermocouples, each of 50 μm diameter and forming a junction approximately 0.1–0.2 mm in diameter, were encased in fused silica tubes of 0.5 mm outer diameter. The thermocouples were scanned by attaching them to a plastic mount that was driven by a stepping motor (rotor SLS-4014-002 model, Princeton, IN) and incremented in steps of 0.1 mm ($\pm$5% per step). A multifunction 16-channel data acquisition system (Labmate Scienmetrics, Nepean, Ontario, Canada) recorded the thermocouple measurements every 1.04 s. The measurements were stored on a personal computer and later analysed. The thermocouples were calibrated in a waterbath against a standard mercury thermometer (Fisher,
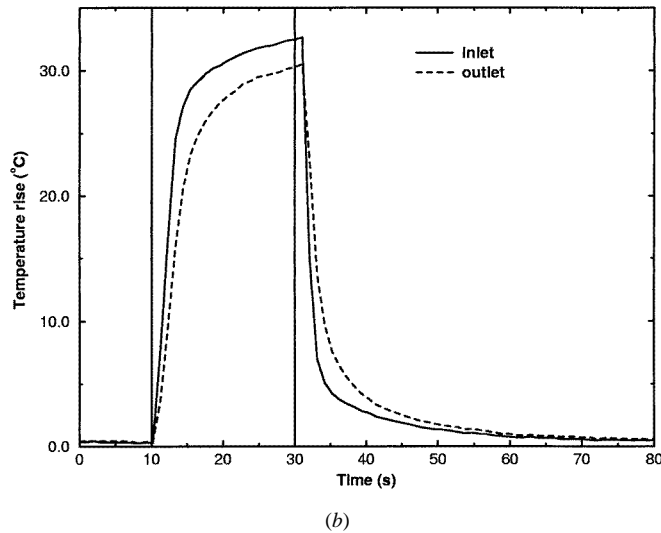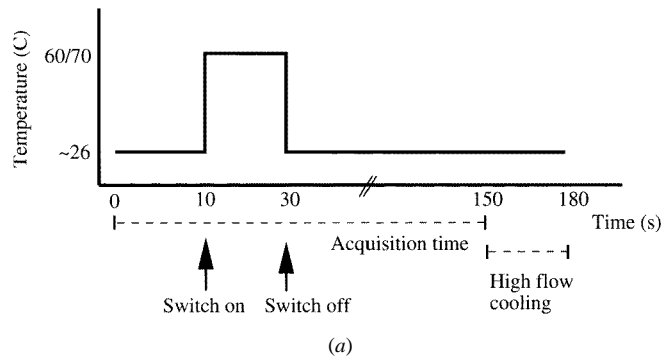
Figure 2. The heating protocol for the transient experiments. (*a*) A 20 s duration pulse of heated water enters the needle and temperature data are collected for 1–2 min. Data acquisition is followed by a 20–30 s 'cooldown' of the kidney. (*b*) Measured temperatures in the pulse heating experiments at the entrance and exit of the needle source. Vertical lines represent pulse on ($t = 10$ s) and off ($t = 30$ s) times.

Canada) and had an accuracy of ±0.1 °C. In the steady state experiments, three temperature measurements were taken at each location and averaged ($\simeq 3$ s per step and 45 min for each scan).

The thermocouple arrangement is shown schematically in figure 3. The locations of the thermocouples were such that one thermocouple path (labelled L(eft) in figure 3) traversed primarily the kidney cortex while the other thermocouples (labelled T(op), M(iddle), B(ottom), R(ight)) traversed both the kidney medulla and cortex. The vascular geometry of the pig kidney suggests that the medulla contains thermally significant and counter-current vessels (Xu *et al* 1994). These thermally significant vessels give rise to arcuate arteries, whose several divisions tend to lie in a plane parallel to the kidney surface at the border between the cortex and the (outer) medulla (Dworkin and Brenner 1991). The kidney cortex has few large vessels, however, and the perfusion in the cortex is more than double that of the medulla. Therefore thermocouple paths T, M, B, R mainly were expected to manifest the effects of thermally significant vessels. The minimum distances of each thermocouple path from the source are tabulated in table 1.

Cross sections through kidney
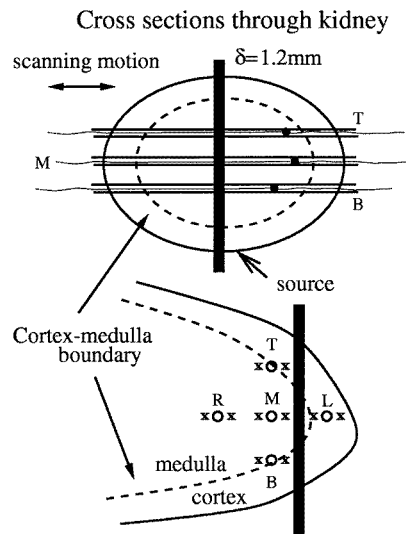
Figure 3. Schematic orthogonal diagrams of thermocouple and source locations in the kidney. Broken lines represent the boundary between the kidney medulla and cortex (outer shell). Locations marked 'x' in the lower portion of the diagram correspond to lines (perpendicular to the plane of the paper) along which CT data are plotted in figures 5(*d*)–(*f*). The thermocouple paths (also perpendicular to the plane of the paper) are denoted by the circles in the diagram.

Table 1. Estimated minimum distance of the thermocouple tracks to the heating needle source measured using CT data.

Thermocouple	Estimated distance (mm)
L	1.2
T	2.0
M	3.3
B	4.2
R	7.3

Thermocouple paths and their separations were determined using high-resolution volumetric x-ray computed tomography (CT) data of the kidney as explained in section 2.2.

To determine if the choice of heating modality affects the flow-induced temperature gradients near the large vessels, the organ was also heated with a distributed ultrasound source. Prior to inserting the needle source into the fixed kidney, the organ was heated using a planar ultrasonic transducer coupled to a conjugate lens (Lalonde *et al* 1993). The conjugate lens is a cross-linked polystyrene lens of variable thickness coupled to the planar transducer, producing multiple foci in the ultrasound field. This transducer lens combination was designed to result in a uniform temperature distribution in perfused tissue (Lalonde and Hunt 1996).

Ultrasound heating required some modifications to the experimental procedure. The water in the waterbath was degassed prior to insonication. A piece of ultrasound absorbing material was placed under the phantom to absorb the ultrasound beam exiting the kidney. A 7 cm diameter planar ultrasound transducer (BSD Medical Corporation, model BSD250, Salt Lake City, UT, USA), operating at 1.45 ± 0.23 MHz, was combined with a conjugate lens to produce nine intensity peaks (FWHM 0.6 mm) in a $2 \times 2 \times 2$ cm focused region. The beam intensity distribution and specific absorption rate are discussed elsewhere (Jia 1995). The focal plane,

located 6 cm from the lens surface, was positioned so as to overlap the plane defined by thermocouples R, M and L. Single temperature measurements were made at each location. Steady state temperature profiles were collected for all five thermocouples for kidney inflows ranging from 0 to 60 ml min^{-1}.

2.2. Computed tomography imaging

Vascular imaging was performed using a high-resolution volumetric CT scanner (Holdsworth *et al* 1990, 1993) to determine the location of large vessels. All experiments were conducted with tube parameters of 80 kVp and 15 mA. Two hundred projections spaced 0.9° apart were collected and used in the CT reconstruction algorithm. The voxel size of the final dataset was 0.4 mm^3. Before data acquisition, the fixed kidney was perfused with water for 10 min and then the flow was stopped. The kidney was then positioned in a plastic container with the five thermocouples and the needle source still attached. Data were collected with and without contrast agent injected in the vasculature. Since acquisition time ranged from 20 to 40 min, a special iodine-based contrast agent (Gazelle *et al* 1994, Wolf *et al* 1994) consisting of radio-opaque nanoparticulates with an average particle size of 250 nm was used to prevent dye leaking from the vasculature. The agent, an ethyl ester of diatriozoic acid (EEDA; Win 8883, Sterling Winthorp Pharmaceutical Research Division, Collegeville, PA) was supplied as a 15% suspension of nanoparticulates (89 mg I/ml). A bolus of the contrast agent was introduced through the renal artery until the agent was detected flowing out of the renal vein. There was no flow through the kidney during data acquisition.

Analysis of the CT dataset was performed using the Explorer data visualization package (NAG, Springfield, IL). Surface renderings were produced to visualize the vascular tree in a three-dimensional representation (figure 4). Thermocouple paths were determined by joining the intersections of the thermocouple trajectories with the kidney surface which were clearly visible in the CT dataset. Artefacts were observed in the CT reconstruction close to the stainless steel needle that made accurate determination of the location of the needle heating source difficult. To compare vessel location to temperature effect, CT data acquired from two locations immediately adjacent and parallel to the thermocouple paths are used (as plotted in figures 5(*d*)–(*f*) and labelled CT-1 and CT-2). These are also marked 'x' in figure 3.

3. Results

3.1. Steady state temperature profiles

Thermally significant vessels have the capacity to redistribute heat by forced convection and thus induce localized temperature gradients in heated tissues. Four of the five thermocouple paths recorded such temperature variations (T, R, M, B). Three quite distinct effects of large vessels were detected during steady state heating (thermocouple paths R, M, B) and are shown in figure 5.

Extended regions of localized cooling were recorded by thermocouple R (figure 5(*a*)). The temperature profile is bell-shaped for no flow, as anticipated for the heating pattern of the cylindrical source. With flow, localized cooling due to the presence of large vessels extends over a region more than 6 mm in length. The temperature profile indicates the presence of at least two thermally significant vessels separated by 2 mm. The effects of the vessels on the temperature profiles are evident even for a very low organ inflow of 0.8 ml min^{-1}. Furthermore, a temperature increase is noted close to the kidney boundary ($x \sim +14$ mm). The location of both temperature fluctuations correlate well with locations of increased pixel intensity in the
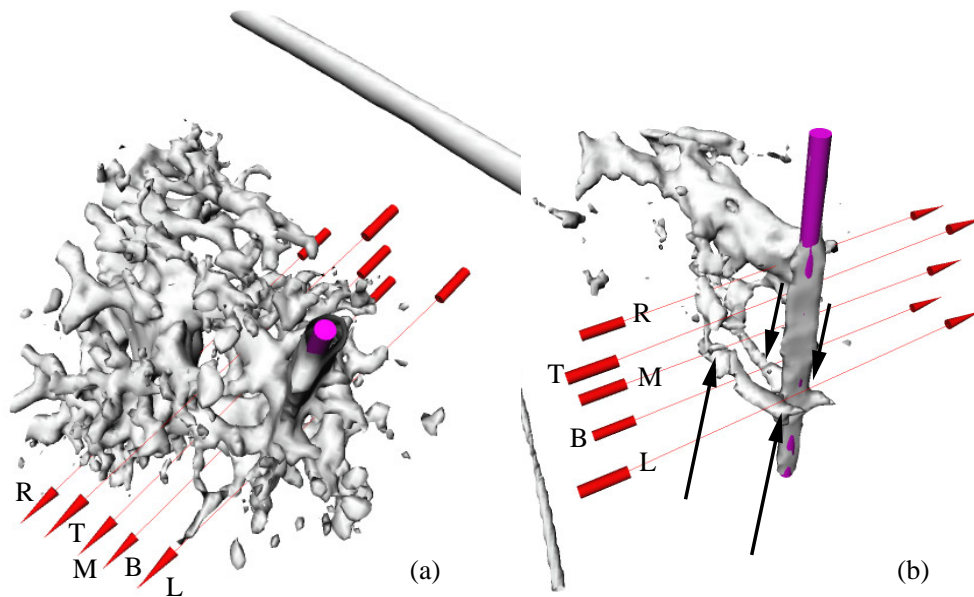
Figure 4. (*a*) Volumetric representation of the kidney vasculature (isosurface value = 145). Labelled arrows indicate the thermocouple paths in the experiments. The solid cylinder represents the needle source (diameter ∼1.2 mm). (*b*) Volumetric representation of the kidney vasculature (isosurface value = 245). A higher value for the isosurface was used to emphasize the larger vessels in the kidney. Arrows indicate locations that large vessel(s) pass near thermocouple paths M (long arrows) and B (short arrows) and the heating source.

CT line profiles (figure 5(*d*)). In this case the vessels caused a significant temperature decrease over an extended region, acting like a strong localized heat sink for high flows. The location of other smaller temperature fluctuations recorded can also be correlated with locations of increased CT intensity (e.g. $x \sim +4$ mm).

Vascular structures can transfer heat from locations close to the heating source to locations further away, causing a localized temperature elevation. This effect, shown in figure 5(*b*), was observed at the location of thermocouple M. The profile is bell-shaped with no flow. With flow, a sharp temperature increase is recorded at a location approximately 1 cm away from the source ($x \sim 6$ mm in the figure). For a kidney inflow of 30 ml min^{-1} this feature dominates the temperature profile inducing steep temperature gradients of 6 °C mm^{-1} (table 2). The CT line profiles in figure 5(*e*) indicate the presence of large vessels at the location at which the temperature peak was measured. Furthermore, the vessel paths detected in figure 4 suggest that the same vessels also pass close to the source. Thus we hypothesize that heat is transferred from a region close to the heating source to the measurement location by the blood vessels resulting in a significant temperature elevation.

Figure 5(*c*) (thermocouple path B) illustrates flow-dependent localized temperature variations caused by a vascular structure hypothesized to be a counter-current pair of vessels. With no flow the temperature curve is bell-shaped. With flow, the peak and valley temperature formation (marked ϵ and δ in the figure) which is characteristic of counter-current flow (van Leeuwen *et al* 1997, Huang *et al* 1996, Baish 1990) is evident. Line profiles extracted from
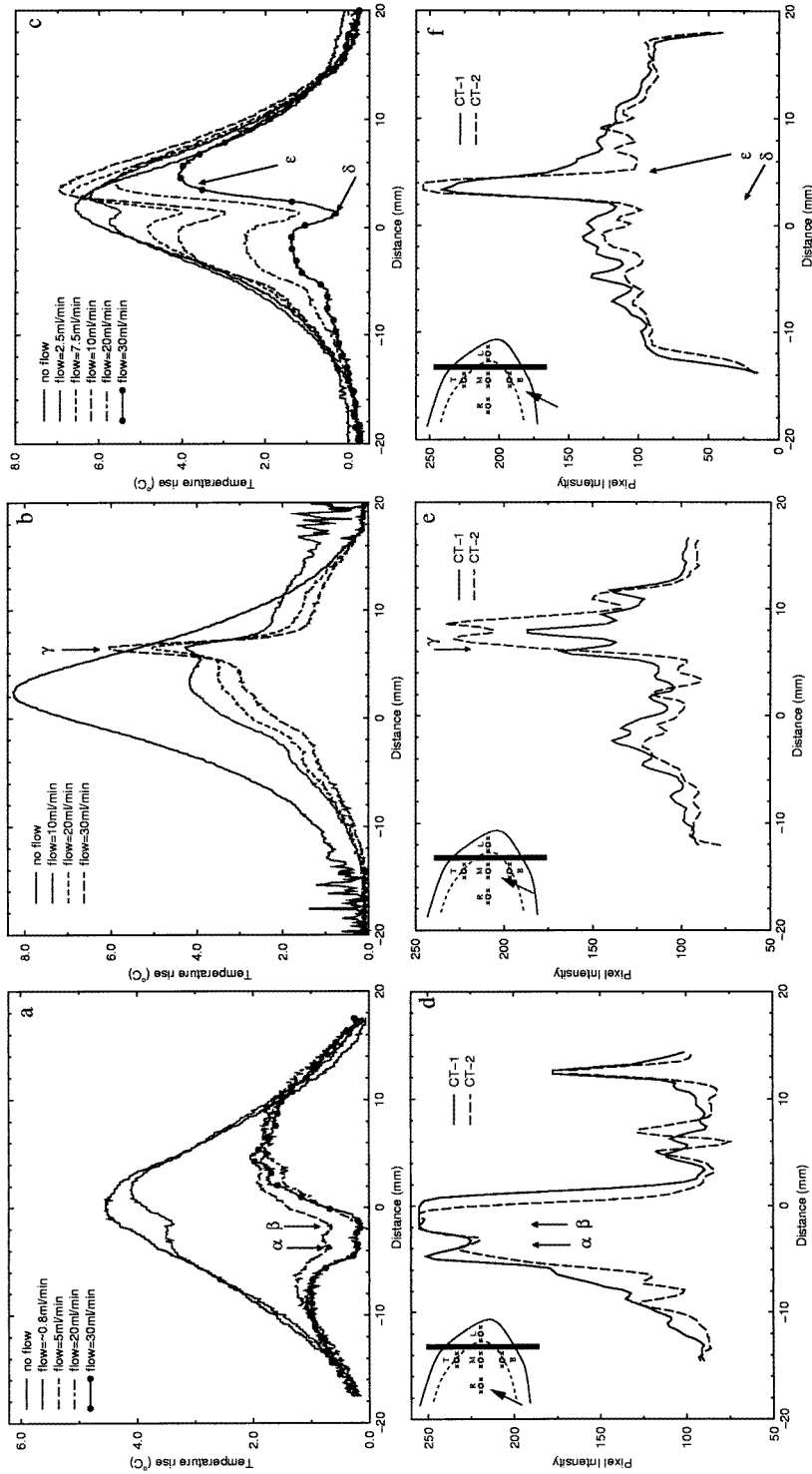
Figure 5. Steady state temperature profiles recorded by thermocouple paths (*a*) R, (*b*) M and (*c*) B as a function of flow. Labelled arrows demonstrate locations of significant localized heating/cooling. Pixel intensity CT data obtained from separate experiments indicating vessel location for thermocouples (*d*) R, (*e*) M and (*f*) B. Arrows in insets of (*d*), (*e*) and (*f*) denote thermocouple location as shown in figure 3. The correspondence of the localized temperature gradients with vessel location based on the imaging data is observed by comparing (*a*) and (*d*), (*b*) and (*e*) and (*c*) and (*f*).

Table 2. Maximum temperature gradient measured at large vessel locations for localized hot water heating.

Flow (ml min^{-1})	Temperature gradient ($^{\circ}$C mm^{-1})	
	Thermocouple B	Thermocouple M
5	0.9	1.2
10	2.3	2.0
20	2.5	3.2
30	2.3	6.0
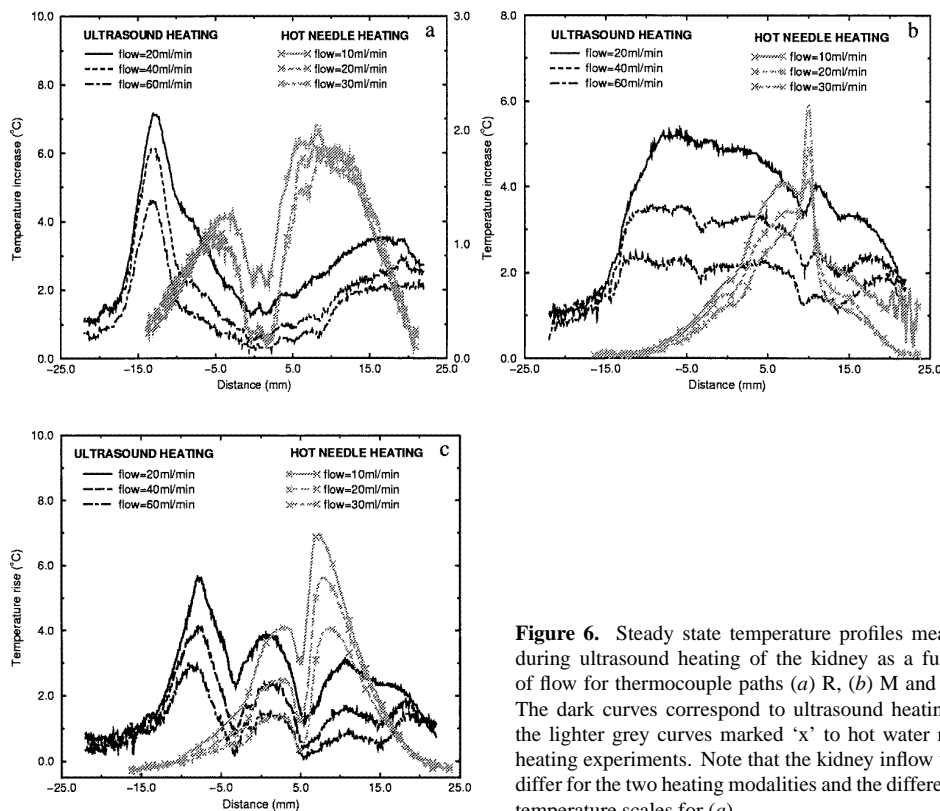
Figure 6. Steady state temperature profiles measured during ultrasound heating of the kidney as a function of flow for thermocouple paths (*a*) R, (*b*) M and (*c*) B. The dark curves correspond to ultrasound heating and the lighter grey curves marked 'x' to hot water needle heating experiments. Note that the kidney inflow values differ for the two heating modalities and the difference in temperature scales for (*a*).

volumetric CT data of the kidney indicate the presence of a vascular structure in this region (figure 5(*f*)). With no flow and a flow of 2.5 ml min^{-1}, the maximum temperature in the profile is *lower* than at 7 and 10 ml min^{-1}. This indicates the dominant role of the vessel that transfers heat to the region for this range of flows. At flows above 10 ml min^{-1} the maximum temperature drops again below the no flow levels, demonstrating that the vessel that transfers heat away from the region dominates. Hence the resultant temperature distribution is a complex function of flow through the two vessels and this vessel structure can heat or cool the adjacent tissues depending on the volumetric flow rate through the vessels and their location with respect to the heating source. The thermal gradients measured close to the vessels were 2–3 $^{\circ}$C mm^{-1} for a kidney inflow of 30 ml min^{-1} (table 2).

Table 3. Maximum temperature gradient measured at large vessel locations for ultrasound heating.

Flow (ml min^{-1})	Temperature gradient ($^\circ$C mm^{-1})	
	Thermocouple B	Thermocouple M
20	1.2	0.8
40	1.5	1.0
60	1.1	1.0

3.1.1. Ultrasound heating. Ultrasound heating of the kidney was performed to examine if the temperature gradients near the large vessels detected with the needle heating source were also observed for a more distributed heating source. Temperature profiles measured for ultrasonic heating of the kidney (section 2) are shown in figure 6. A larger volume of the kidney was heated as compared with the highly localized heating by the hot water needle source. With kidney perfusion, temperature variations similar to those measured in section 3.1 were detected. The distinct effects of large vessels using this method of heating are shown in figure 6.

The steady state temperature profiles recorded by thermocouples R, M and B for the ultrasound heating experiments are plotted in figures 6(*a*), (*b*) and (*c*) respectively. Superimposed on this figure are the temperature profiles (grey lines) that correspond to the hot water heating experiments of figure 5. This allows direct comparison of the distributions by the two heating methods. Since there was no common frame of reference between the two experiments, profiles were shifted to match localized features using the temperature profiles recorded by thermocouple path R as a reference (figure 6(*a*)).

For thermocouple R the extensive region of cooling was coincident for both heating modalities (figure 6(*a*)). The temperature gradients measured close to the large vessels for ultrasound heating were not as steep as the gradients for the needle heating.

Significant differences in the effects of large vessels on the temperature distributions for the two heating methods were recorded by thermocouple M (figure 6(*b*)). In this case the region of localized heating observed in the hot water heating experiments (figure 5(*b*)) corresponded to a region of localized cooling in the ultrasound experiments. The extent of the cooling/heating due to the vessel structure was approximately 1 mm for the flow rate of 20 ml min^{-1} for both ultrasound and hot water heating (as measured by the width of the dip or peak). The maximum temperature gradient measured at the location of the vessels, while fairly insensitive to flow for the ultrasound experiments, changed by up to a factor of four for the range of flows used in the hot water experiments (table 3). The steepest temperature gradients measured in the case of ultrasonic heating were 1.2 $^\circ$C mm^{-1}, a factor of four less than those recorded with needle heating for comparable temperature rises at that location.

The locations of the flow-induced temperature fluctuations measured by thermocouple B during ultrasound heating were coincident with the locations recorded in the hot water experiments (figure 6(*c*)). In this case, however, the counter-current nature of the vessels is not as evident since there is less excess heating adjacent to the region of cooling (locations δ and ϵ in figure 5(*c*)). Furthermore, the temperature gradients between the vessels were not as steep and not as sensitive to kidney inflow changes when compared with the needle heating (table 3). The data recorded by thermocouples M and B illustrate that the heating method influences the way large vessels perturb the temperature field.
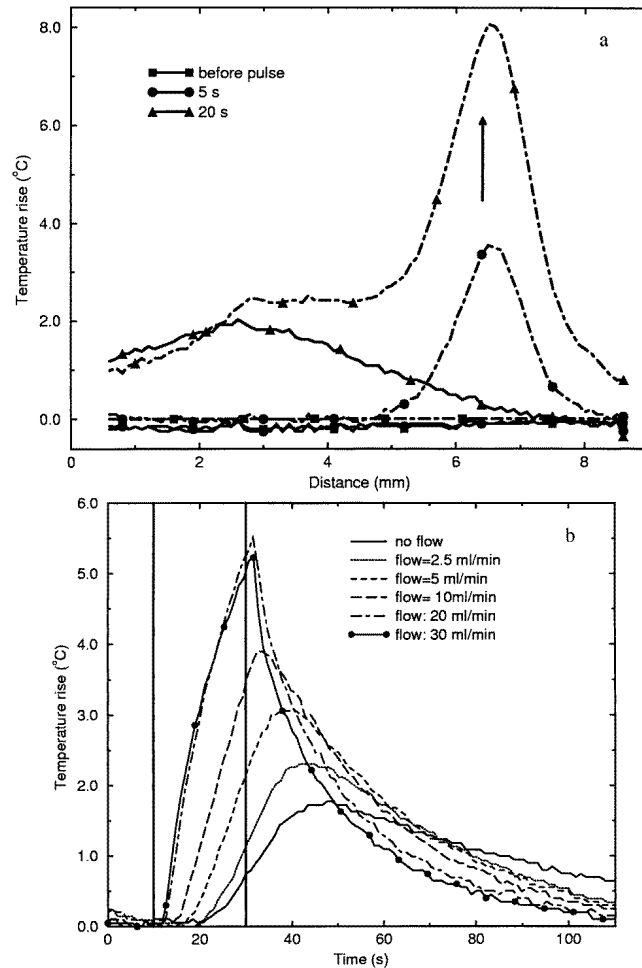
Figure 7. Temperature profiles recorded by thermocouple M as a function of distance recorded at three different times (before pulse, 5 s and 20 s after pulse is on) without flow (solid curve) and with a kidney inflow of 30 ml min^{-1} (dot-dashed curve). Arrow denotes location at which the data in (*b*) were collected. (*b*) Transient temperature profiles recorded by thermocouple M as a function of kidney inflow (at the location shown by the arrow in panel (*a*) of this figure and in figure 5(*b*)). The maximum temperature reached increases sixfold in comparison with the no flow case and the delay time is reduced by 20 s. Vertical lines indicate source 'on' (*t* = 10 s) and 'off' (*t* = 30 s) times.

3.2. Transient temperature profiles

Transient heating experiments were performed to examine how the presence of large vessels perturbs tissue temperature profiles during short-duration high-temperature thermal therapies and how the temperature profiles compare to those recorded during steady state heating at the same locations. Figures 7 and 8 represent the temperature profiles measured by thermocouples M and B respectively. Due to the large distance separating thermocouple R from the source (a minimum of 7.3 mm), the tissue temperature increase at this location was less than 0.3 °C and thus the data are not presented.
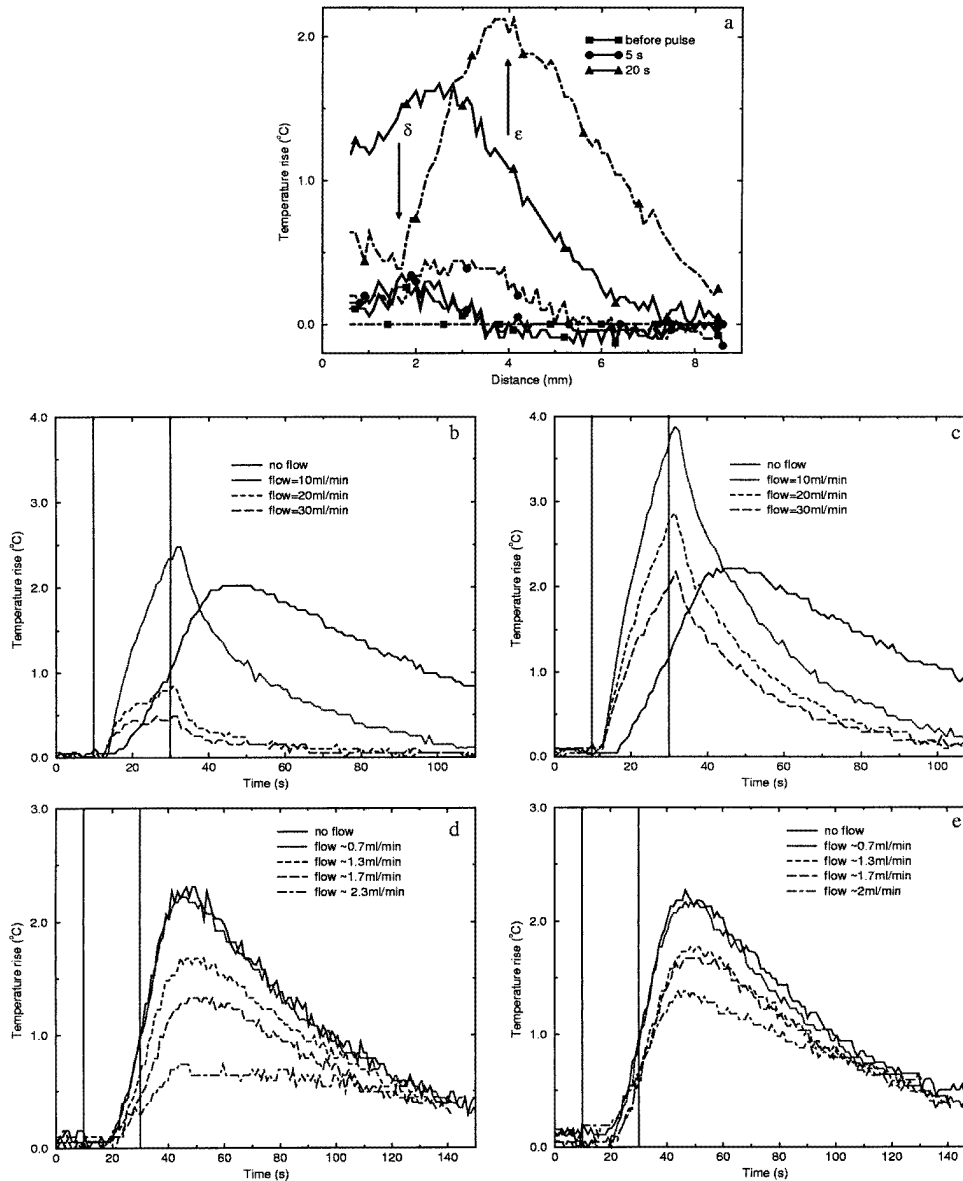
Figure 8. (*a*) Temperature profiles recorded by thermocouple B as a function of distance at three different times (before the pulse, 5 s and 20 s after the hot water pulse started) without flow (solid curve) and with a kidney inflow of 30 ml min^{-1} (dot-dashed curve). Arrows indicate location of temperature/time plots shown in (*b*) and (*d*) (downward arrow, location δ) and (*c*) and (*e*) (upward arrow, location ϵ). Panels (*b*) and (*c*) represent profiles measured with high kidney flows ($T_{in} \sim 33\,°C$) while (*d*) and (*e*) represent profiles for low flows ($T_{in} \sim 38.5\,°C$). Vertical lines indicate source 'on' ($t = 10$ s) and 'off' ($t = 30$ s) times. Note the difference in scales in (*b*), (*c*) and (*d*), (*e*).

Figure 7(*a*) shows the temperatures recorded along an 8 mm track of thermocouple path M that includes the region of localized heating detected in the steady state experiments (figure 5(*b*)). Before the pulse, the temperature profiles were relatively flat indicating that

the kidney had cooled back to the ambient temperature in all pulsed experiments before the start of the next heating pulse. For no flow, a portion of the bell-shaped temperature curve can be distinguished at the end of the pulse. With flow, a dramatic change in the temperature profile is detected at the location where localized heating was detected in figure 5(*b*). Even at times as short as 5 s after the pulse, the effects of flow on the temperature distribution are significant. The extent of the localized heating is consistent with the steady state temperature profiles with respect to the location along the scanning path and the extent of heating (peak full-width half-maximum ∼1 mm). Figure 7(*b*) illustrates the transient profiles measured with thermocouple M at the location shown by the arrow in figures 5(*b*) and 7(*a*). For a kidney inflow of 30 ml min^{-1} the maximum temperature was six times greater than that of the no flow case. Furthermore, the time between the start of the heat pulse and the first recorded temperature rise (hereafter referred to as the delay time) was reduced by 20 s. The increase in the maximum temperature and reduction in the delay time imply heat transferred from one region to another by convective heat transfer. The imaging data of figure 4(*b*) further support this hypothesis (long arrows). The large vessel(s) highlighted pass close to the source and thermocouple path M. Thus the effects of large vessels on the temperature distributions are significant, even for short heating times, and the magnitude of the effects decreases as flow is reduced.

The transient temperature response close to the hypothesized counter-current vessel structure is shown in figure 8 for a range of flows. Temperatures were recorded along an 8 mm path of thermocouple path B which includes the location that the temperature peak and valley were detected in the steady state experiments (figure 5(*c*)). With no flow, a portion of the bell-shaped profile is seen at 20 s after the pulse is turned on (figure 8(*a*)). With flow two notable features in the profiles are observed, particularly at the 20 s timepoint: (a) the transfer of heat to the region labelled ϵ (accounting for the increase in temperature in the region when compared to the no flow data) and (b) the removal of heat from the location labelled δ (accounting for the excess cooling). These results are consistent with the observations from the steady state experiments: with flow higher temperatures were recorded at location ϵ and lower temperatures at location δ with respect to the no flow data. A large vessel (or a collection of vessels that could not be resolved) crosses both thermocouple path B and the source as shown in figure 4(*b*) (short arrows). Convective heat transfer by these vessels may account for the temperature peak detected at location ϵ (as the peak for thermocouple path M).

The flow dependence of the temperature profiles reveals the dynamics of heat transfer close to these vessels. The transient temperature profiles at locations δ and ϵ are presented in figures 8(*b*) and (*c*) for high flows and 8(*b*) and (*d*) for low flows. With no flow the two temperature profiles at δ and ϵ are similar due to the proximity of the two locations (separated by ∼2 mm). With flow, the delay time at location ϵ decreased and the maximum temperature increased with respect to the no flow values (figure 8(*c*)). These changes imply heat transfer to the region by blood flow convection. As flow was increased from 10 to 30 ml min^{-1}, the delay time remained unchanged and the maximum temperature decreased. This is consistent with the steady state temperature profile observations for which the maximum temperature recorded at location ϵ peaked for a flow of 10 ml min^{-1}, decreasing for higher flows. We hypothesize that this decrease with flow is due to increased cooling from the vessel near location δ and/or less efficient convective heat transfer to location ϵ. Heat transfer between these vessels accounts for the fact that even though the vessel near location δ removes heat from the region, the delay time in the temperature profile at that location is reduced (there is a lag of 1–2 s with respect to the delay time measured at location ϵ). The reduction in the delay time at location δ implies heat transfer between the two vessels upstream from the thermocouple and heating source location, as explained in the discussion.

The transient data at locations δ and ϵ exhibit a different behaviour for very low kidney inflows (up to 2.3 ml min^{-1}). For this range of flows the maximum temperature decreased and the delay time was virtually unaffected as flow increased at both locations (figure 8(d) and (e)). Convective heat transfer by the vessel that passes location ϵ could not increase the maximum temperature (with respect to no flow) nor decrease the delay time. This is consistent with the observation in the steady state experiments that for a kidney inflow of 2.5 ml min^{-1} the temperature at location ϵ decreased with respect to no flow. Also of note is the observation that the cooling rates after the end of the pulse *decreased* at these locations as flow increased. For higher flows the maximum temperature increases (before decreasing again) and the delay time decreases (figure 8(c)). The data indicate that heat transfer between the two vessels determines the temperature distribution in the region and that the dynamics of this process are a complex function of flow.

4. Discussion

For the first time, temperature gradients created by large vessels were measured as a function of organ inflow for both steady state and transient heating. This study demonstrates that thermally significant vessels can either cool or heat tissues (figures 5(a) and 5(b) respectively) and that these effects are a complex function of the vessel diameter and volumetric flow through the vessel(s), the proximity of the vessel(s) to the heating source and the choice of heating modality. For example, the vessels in figure 5(b) ($x \sim 6.5$ mm) did not induce large localized gradients for lower flows but did for higher flows and the paired vessels in figure 5(c) ($x \sim 4$ mm) caused an increase in temperature for lower flows and a decrease for higher flows (when compared with the no flow profiles). Furthermore, one can conclude that knowledge of vessel geometry alone is inadequate to predict temperature profiles since knowledge of the flow rate is essential (figures 5 and 7). Simple bioheat transfer models such as the Pennes bioheat transfer equation (BHTE) and effective thermal conductivity equation (ETCE), which in general are not used to model large vessel heat transfer, could not predict the temperature profiles recorded in these experiments. However, in regions where thermally significant vessels were not detected (thermocouple path L in these experiments), the BHTE was found to accurately model the measured temperature distributions (Kolios *et al* 1998).

Thermally significant vessels can lead to excess heating or cooling, even for short heating times. Significant localized heating caused by large vessel(s) (figure 7) was detected as early as 3 s after the start of the heating pulse and persisted until steady state was achieved. The imaging data in figure 4(b) show a vessel at a short distance from both the thermocouple path and the heat source. Simple thermal models that do not take these vessel(s) into account do not predict the excess heating observed in figure 7. These effects are reduced as kidney inflow decreases, as predicted theoretically (Kolios *et al* 1995). Therefore, even for short-duration thermal therapies for which the effects of perfusion are minimized (Billard *et al* 1990, Kolios *et al* 1996), thermally significant vessels should be accounted for. The vessel flow rate is not known in these experiments. However, it can be shown that the average velocity through the vessel is proportional to the input volumetric flow rate of the organ (West *et al* 1997). Therefore, changes in the kidney inflow should correspond to vessel flow rate changes.

While most temperature fluctuations were similar for both hot water and ultrasound heating (i.e. regions of either cooling or heating close to vessels), there were notable exceptions. The region of localized heating in the hot water heating experiment shown in figure 5(b) corresponds to a region of localized cooling in the ultrasound experiment (figure 6(b)). This suggests that the mechanism of heating can influence the temperature gradients caused by large vessels. In the ultrasound experiments, a large volume of tissue is heated compared with needle heating.

Therefore blood may be pre-heated, inducing smaller blood flow related temperature gradients. Furthermore, the maximum temperature gradients caused by the thermally significant vessels were fairly insensitive to kidney inflow for ultrasound heating (table 3) but increased as a function of flow for the needle heating experiments (table 2). During thermal therapies, regions with steep temperature gradients caused by large vessels would be more difficult to heat and would require heating devices with very good local power control to compensate for the heat loss/gain in the region.

Good spatial correlation was obtained when comparing the locations of large vessels derived from the CT experiments and the locations of enhanced cooling or heating measured in the temperature profiles. Furthermore, comparable features were detected at locations with thermally significant vessels for the steady state and transient heating experiments. In general, regions where the temperature increased with flow in the steady state profiles (figures 5(*b*) and 5(*c*)) correspond to transient temperature profiles with reduced delay times, increased maximum temperatures and increased cooling rates when compared with the profiles without kidney flow (figures 7(*b*) and 8(*c*)). Thermally significant vessels that pass close to the heating source transfer heat to the region of increasing the local tissue temperature. This should occur provided that (a) the distance between the vessel and the source and (b) the flow rate through the vessels are sufficient for heat from the source to increase the blood vessel temperature. After the pulse, an increased cooling rate would be anticipated since the vessel transports heat away by convection. Conversely, regions where the temperature decreased in the steady state temperature profiles with flow (figures 5(*a*) and 5(*c*)) correspond to transient temperature profiles with a reduced temperature rise in comparison with the no flow case (figure 8(*b*)) and increased cooling.

In the pulsed experiments the temperatures recorded at location δ (figure 8) follow the same trends for low flows, but for higher flows they diverge. For the low flow range the cooling rates decrease as flow increases (figures 8(*d*) and (*e*)). These results are difficult to reconcile with simple models of bioheat transfer. The strong coupling of the temperature profiles suggest that they are caused by a counter-current pair of vessels. One simplified conceptual model that can qualitatively explain the results is presented in figure 9. Heat emanating from the source increases the blood temperature in the second vessel that causes the temperature increase at location ϵ to convective heat transfer. Perfusate flowing in the opposite direction causes the cooling at location δ. At higher flows, the cooling dominates the region reducing the heat convected to region ϵ. Heat exchange distal to the source can account for the reduction in delay time at location δ in the transient experiments (figure 8(*b*)). The complex temperature profiles near these vessels demonstrate that thermal models should include this feature of the vascular system to accurately model temperature distributions. In figure 4(*b*) (short arrows) a vascular structure that passes by both thermocouple path B and the heating source is shown. This structure may be a counter-current pair of vessels that the imaging experiments could not adequately resolve. The dynamics of counter-current flow and their effect on the temperature profiles may be especially important in cases of vasodilation/vasoconstriction caused either by external pharmacological agents or the heating itself.

This experimental system allowed a detailed examination of the flow-dependent temperature profiles of a heated, perfused kidney for both steady state and transient heating protocols. Such experiments are difficult to perform *in vivo* since data acquisition time is long (several hours) and experimental parameters (such as organ inflow) are difficult to control. Furthermore, organ motion and dynamic vascular changes during heating would contribute to temperature variations during experiments. The fixed kidney model, however, allowed temperature measurements under controlled conditions. Fine spatial step increments (0.1 mm) and thus the measurement of temperature gradients of up to $6\,°\text{C}\,\text{mm}^{-1}$ were achieved
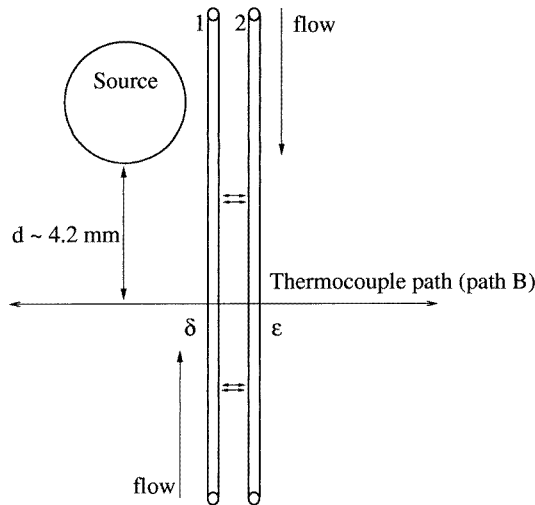
Figure 9. Schematic diagram of counter-current vessel pair model used to interpret the temperature profiles measured by thermocouple B. The labels δ and ϵ denote the locations of the temperature valley and peak in the measured temperature profiles of figures 5(*c*) and 8(*a*). Horizontal arrows signify heat exchange between vessels 1 and 2.

repeatedly. Temperature smearing due to thermocouple conductivity and the quartz tubing was minimized by using type K thermocouples (Gerig *et al* 1992, Brown *et al* 1992) scanned through fixed, small-outer-diameter quartz tubing. These localized temperature gradients may not be adequately resolved during hyperthermia treatments or animal experiments in which the spatial sampling is of the order of 0.5 to 1 cm. Furthermore, the large catheters used clinically 'smear' the temperature gradients (Gerig *et al* 1992, Valvano and Yuan 1992) and thus underestimate the effects of the spatial variation of perfusion and of large vessels. Despite these limiting factors, similar blood flow induced temperature gradients have been observed in human hyperthermia treatments (Levin *et al* 1994).

Large vessel effects must be accounted for when planning thermal therapy treatments. This is important when critical regions close to large vessels are to be treated or spared. Heating modalities that rely on conduction to heat large volumes, thus creating steep temperature gradients (such as interstitial laser photocoagulation (Wyman *et al* 1992) and other interstitial techniques) are particularly vulnerable to these effects. The challenge is to incorporate large vessel geometry and flow in thermal models for treatment planning. Several groups are working on this problem (Kotte *et al* 1996, Rawnsley *et al* 1994, Dutton *et al* 1993). Current imaging technologies allow vessels of at least 1 mm diameter to be detected *in vivo* and thus treatment planning could take into account some of the thermally significant vessels in the treatment field.

5. Conclusions

A very good correlation between the locations of thermally significant vessels as determined by computed tomography and temperature fluctuations in a perfused fixed heated kidney was obtained. It was shown that large vessels can heat as well as cool tissues and that these effects depended on the vessel location with respect to the heating source and the type of heating source used. It was demonstrated in a well controlled experimental system that temperature gradients

caused by thermally significant vessels depend on the volumetric flow rates through the vessels and that knowledge of vascular geometry alone is not sufficient to predict the effects of large vessels on the temperature distribution. Furthermore, these temperature gradients are steeper and more sensitive to flow variations for localized heating techniques when compared with more distributed sources. The need to include counter-current vessel heat transfer in bioheat transfer models was also illustrated. The transient tissue temperature distributions measured during pulsed heating of the kidney were consistent with the steady state profiles. Regions close to thermally significant vessels where the temperature increased with flow in the steady state profiles correspond to transient temperature profiles with reduced delay times, increased maximum temperatures and increased cooling rates when compared to the profiles without kidney flow. Conversely, regions close to thermally significant vessels where the temperature decreased in the steady state temperature profiles correspond to transient temperature profiles with a reduced temperature rise and increased cooling rates as a function of flow when compared to the profiles without kidney flow. Finally, it was shown that even for very short treatment times, large vessels can have significant effects on the temperature profiles and must be included in treatment planning. These effects are minimized when flow through the vessels is reduced.

Acknowledgments

References

Arkin H, Xu L X and Holmes K R 1994 Recent developments in modeling heat transfer in blood perfused tissues *IEEE Trans. Biomed. Eng.* **41** 97–107

Baish J W 1990 Heat transport by countercurrent blood vessels in the presence of an arbitrary temperature gradient *J. Biomech. Eng.* **112** 207–11

Billard B E, Hynynen K and Roemer R B 1990 Effects of physical parameters on high temperature ultrasound hyperthermia *Ultrasound Med. Biol.* **16** 409–20

Brown S L, Li X L, Pai H H, Hill R P and Hunt J W 1992 Observations of thermal gradients in perfused tissues using water bath heating *Int. J. Hyperth.* **8** 275–87

Chato J C 1980 Heat transfer to blood vessels *J. Biomech. Eng.* **102** 110–18

Crezee J and Lagendijk J J W 1990 Experimental verification of bio-heat transfer theories: measurement of temperature profiles around large artificial vessels in perfused tissue *Phys. Med. Biol.* **35** 905–23

——1992 Temperature uniformity during hyperthermia: the impact of large vessels *Phys. Med. Biol.* **37** 1321–37

Damianou C A, Hynynen K and Fan X 1995 Evaluation of accuracy of a theoretical model for predicting the necrosed tissue volume during focused ultrasound surgery *IEEE Trans. Ultrasonics Ferroelectrics Frequency Control* **42** 182–7

Dorr L N and Hynynen K 1992 The effects of tissue heterogeneities and large vessels on the thermal exposure induced by short high-power ultrasound pulses *Int. J. Hyperth.* **8** 45–59

Dutton A, Darkazanll A, Heinrch J C and Roemer R B 1993 Finite element solution to conjugated heat transfer tissue using magnetic resonance angiography to measure *in vivo* flow *ASME Adv. Heat Mass Transfer* 101–6

Dworkin L D and Brenner B M 1991 *The Kidney* 4th edn (Philadelphia: Saunders) pp 164–204

Gazelle G S, Wolf G L, Bacon E R, McIntire G L, Cooper E R and Toner J L 1994 Nanocrystalline computed tomography contrast agents for blood-pool and liver-spleen imaging *Invest. Radiol.* **29** (suppl 2) S286–8

Gerig L H, Szanto J and Raaphorst G P 1992 On the spatial resolution of clinical thermometers *Med. Phys.* **19** 679–84

Hand J W, Machin D, Vernon C C and Whaley J B 1997 Analysis of thermal parameters obtained during phase III trials of hyperthermia as an adjunct to radiotherapy in the treatment of breast carcinoma *Int. J. Hyperth.* **13** 343–64

Hill C R, Rivens I, Vaughan M G and ter Haar G R 1994 Lesion development in focused ultrasound surgery: a general model *Ultrasound Med. Biol.* **20** 259–69

Holdsworth D W, Drangova M and Fenster A 1993 A high-resolution XRII-based quantitative volume CT scanner *Med. Phys.* **20** 449–62

Holdsworth D, Drangova M, Schulenburg K and Fenster A 1990 A table-top CT system for high resolution volume imaging *Proc. SPIE* **1231** 239–43

Holmes K R, Ryan W, Wienstein P and Chen M M 1984 A fixation technique for organs to be used as perfused tissue phantoms in bioheat transfer studies *ASME Adv. Bioeng.* 9–10

Huang H W, Chen Z P and Roemer R B 1996 A counter current vascular network model of heat-transfer in tissues *J. Biomech. Eng.* **118** 120–9

Jia Z Q 1995 Temperature homogeneity and blood flow in renal hyperthermia *Master's Thesis* University of Toronto

Kapp D S 1996 Efficacy of adjuvant hyperthermia in the treatment of superficial recurrent breast cancer: confirmation and future directions *Int. J. Radiat. Oncol. Biol. Phys.* **35** 1117–21

Kapp D S and Cox R S 1995 Thermal treatment parameters are most predictive of outcome in patients with single tumor nodules per treatment field in recurrent adenocarcinoma of the breast *Int. J. Radiat. Oncol. Biol. Phys.* **33** 963–4

Kolios M C, Sherar M D and Hunt J W 1995 Large vessel cooling in heated tissues: a numerical study *Phys. Med. Biol.* **40** 477–94

——1996 Blood flow cooling and ultrasonic lesion formation *Med. Phys.* **23** 1287–98

Kolios M C, Sherar M D, Worthington A E and Hunt J W 1994 Modeling temperature gradients near large vessels in perfused tissues *Fundamentals of Biomedical Heat Transfer* ed M A Ebadian and P H Oosthuizen (American Society of Mechanical Engineers) pp 23–30

Kolios M C, Worthington A E, Sherar M D and Hunt J W 1998 Experimental evaluation of two simple thermal models using transient temperature analysis *Phys. Med. Biol.* **43** 3325–40

Kotte A, Van Leeuwen G, Debree J, Vanderkoijk J, Crezee H and Lagendijk J 1996 A description of discrete vessel segments in thermal modeling of tissues *Phys. Med. Biol.* **41** 865–84

Lagendijk J J W 1982 The influence of blood flow in large vessels on the temperature distribution in hyperthermia *Phys. Med. Biol.* **27** 17–23

Lalonde R J and Hunt J W 1996 Optimizing ultrasound focus distributions for hyperthermia *IEEE Trans. Biomed. Eng.* **42** 981–90

Lalonde R J, Worthington A E and Hunt J W 1993 Field conjugate acoustic lenses for ultrasound hyperthermia *IEEE Trans. Ultrasonics Ferroelectrics Frequency Control* **29** 495–507

Levin W, Sherar M D, Cooper B, Hill R P, Hunt J W and Liu F F 1994 The effect of vascular occlusion on tumor temperatures during superficial hyperthermia *Int. J. Hyperth.* **10** 495–505

Raaymakers B W, Crezee J and Lagendijk J J W 1998 Comparison of temperature distributions in interstitial hyperthermia: experiments in bovine tongues versus generic simulations *Phys. Med. Biol.* **43** 1199–214

Rawnsley R J, Roemer R B and Dutton A W 1994 The simulation of discrete vessel effects in experimental hyperthermia *J. Biomech. Eng.* **116** 256

Roemer R B 1991 Optimal power deposition in hyperthermia I. The treatment goal: the ideal temperature distribution II. The role of large blood vessels *Int. J. Hyperth.* **7** 317–41

Sherar M D *et al* 1997 Relationship between thermal dose and outcome in thermoradiotherapy treatments for recurrences of breast cancer: data from a phase III trial *Int. J. Radiat. Oncol. Biol. Phys.* **39** 371–80

Valvano J W and Yuan D Y 1992 Quantification of errors occurring when measuring spatially-varying temperatures *ASME Adv. Bio. Heat Mass Transfer* 39–45

van Leeuwen G M, Kotte A N C J and Lagendijk J J W 1997 Tests of the geometrical description of blood vessels in a thermal model using counter-current geometries *Phys. Med. Biol.* **42** 1515–32

West G B, Brown J H and Enquist B J 1997 A general model for the origin of alliometric scaling laws in biology *Science* **276** 122–6

Wolf G, Gazelle G, McIntire G, Bacon E, Toner J, Cooper E and Haley P 1994 Percutaneous computed tomography lymphography in the rabbit by subcutaneously injected nanoparticulates *Acad. Radiol.* **1** 352–7

Wyman D R, Whelan W M and Wilson B C 1992 Interstitial laser photocoagulation: Nd:YAG 1064 nm optical fiber source compared to point heat source *Lasers Surg. Med.* **12** 659–64

Xu L X, Holmes K R, Moore B, Chen H and Arkin M M 1994 Microvascular architecture within the pig kidney cortex *Microvasc. Res.* **47** 293–307